Expanded View Figures

Figure EV1. The role of Jacob in cAMP-responsive element-binding protein (CREB) shutoff.

A Validation of Jacob and pJacob antibodies for detection of the human protein. Human Jacob fused to a Spot tag was expressed in HEK293T cells for antibody detection. The rat amino acid sequence of Jacob used for generation of pan-Jacob antibodies is highly conserved in human and mouse and the antibody effectively detects human Jacob.

B, C Total Jacob protein levels are not significantly reduced in brain samples from Alzheimer's disease (AD) patients as compared to the control group. (C) Bar plots representing the quantification of Jacob immunoreactivity normalized to H3. $N = 11$–12 protein extracts from different subjects in each group.

D, E Total NeuN protein levels are significantly reduced in brain samples from AD patients as compared to the control group. (C) Bar plots representing the quantification of NeuN immunoreactivity normalized to H3. $N = 11$–12 protein extracts from different subjects in each group.

F Scatter plots representing gating strategy used in FACS experiments for neuronal pCREB and CREB immunoreactivity quantification.

G, H Acute (1 h) $A\beta_{1\text{-}42}$ treatment does not induce changes in pan CREB levels in organotypic hippocampal slices from Jacob (−/−) mice. (G) Representative confocal images of slices immunolabeled against pCREB, co-labeled with NeuN and DAPI. Scale bar: 100 μm. (H) Bar plot of CREB immunoreactivity averaged per slice, $N = 14$–16 slices.

I pJacob level and pJacob/panJacob ratio are decreased in TBA2.1 mouse line compared to WT animals. Representative images of the immunoblot probed with antibodies against pJacob, pan-Jacob, and re-probed with Histone3 (H3).

J–L Bar plots representing the quantification of (J) Jacob, (K) pJacob levels and the (L) pJacob/Jacob ratio normalized to H3. $N = 5$–7 hippocampal protein extracts.

M Significant changes in cerebral blood flow between TBA2.1 and WT, TBA2.1, −/− and WT, and TBA2.1 and TBA2.1, −/− as determined by 99mTc-HMPAO SPECT measurements. Difference images overlay over a reference MR for comparison with TBA2.1 mice as described on panel labeling. Bregma −2.5. Statistically significant differences between TBA2.1 and double transgenic animals were detected in dorsal CA1 (regions indicated by arrowheads). $N = 10$ animals ($P < 0.05$) by two-tailed Student's *t*-test.

N Significant changes in cerebral blood flow between TBA2.1 and WT, TBA2.1, −/− and WT as determined by SPECT measurements. Statistically significant differences between TBA2.1 or double transgenic animal and WT were detected in lateral septal nucleus and the diagonal band nucleus (regions indicated by arrowheads) ($P < 0.01$) by two-tailed Student's *t*-test.

O–Q The quantification of glial cells revealed no major differences between TBA2.1 and double transgenic animals (TBA2.1, −/−). (O) Representative confocal images of distal CA1 sections from 13 weeks old mice stained for GFAP, DAPI and Iba-1. Scale bar: 100 μm. (P) Bar plot representing the number of GFAP-positive cells per rectangular region of interest. $N = 17$–24 cryosections from 5 to 7 animals per genotype. (Q) Bar plot representing the number of Iba-1-positive cells per rectangular region of interest. $N = 17$–26 cryosections from 5 to 7 animals per genotype.

R, S The quantification of Aβ plaques revealed no major differences between TBA2.1 and double transgenic animals (TBA2.1, −/−). (R) Confocal images averaged from two sections of the molecular layer of 13-week-old mice distal CA1 labeled for amyloid-β (4G8 antibody) and co-stained with DAPI. Scale bar: 100 μm. (S) Bar plot representing the number of amyloid-β-positive puncta per 100 μm. $N = 8$, number of cryosections from two animals per genotype.

Data information: ns, non-significant difference, $^*P < 0.05$, $^{**}P < 0.01$, $^{***}P < 0.001$ by (C, J–L) two-tailed Student's *t*-test or (H) two-way ANOVA followed by Bonferroni's multiple comparisons test or (P, Q, S) linear mixed-effects model followed by Tukey's multiple comparisons test. All data are represented as mean ± SEM.
Source data are available online for this figure.

© 2023 The Authors

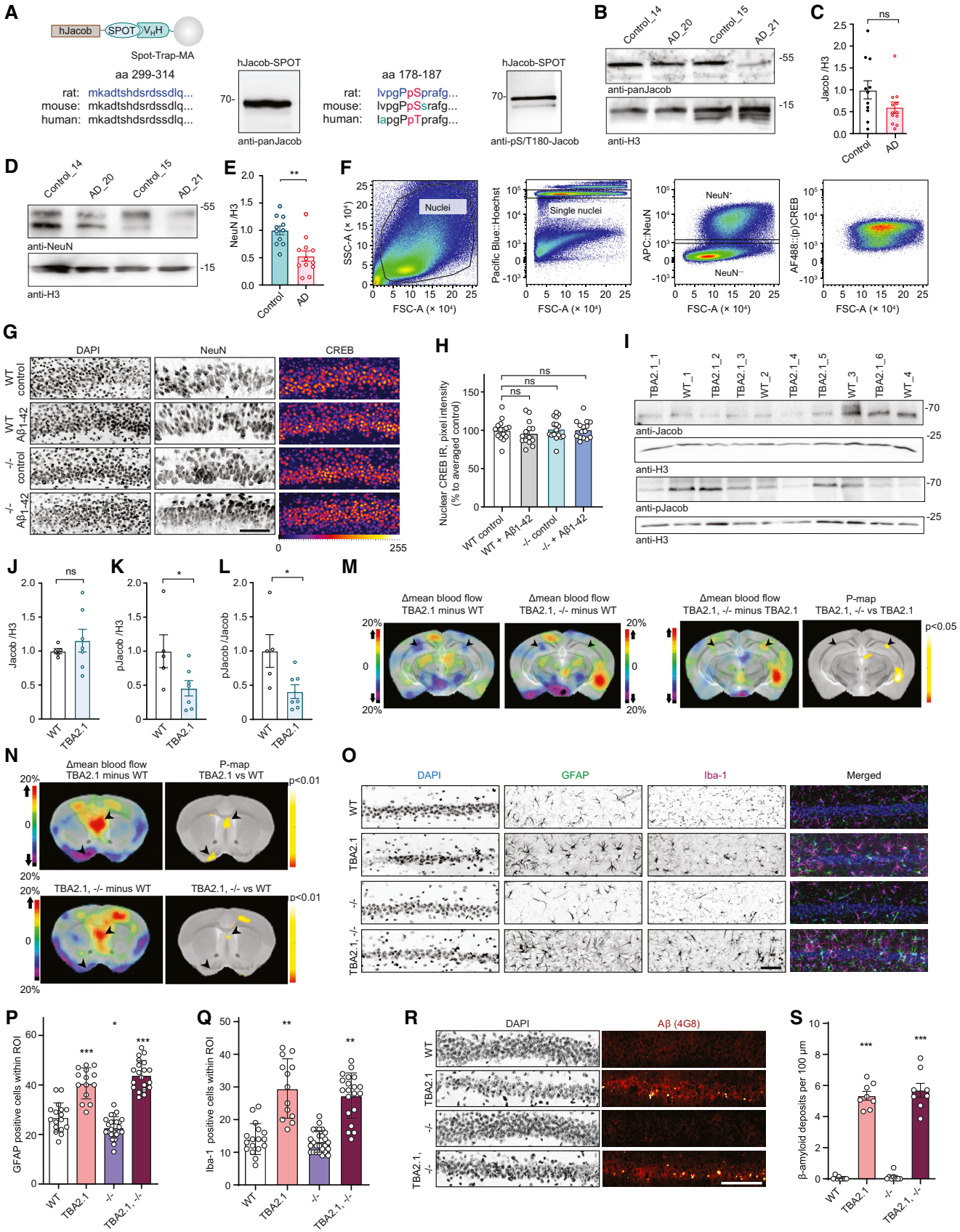

Figure EV1.

© 2023 The Authors

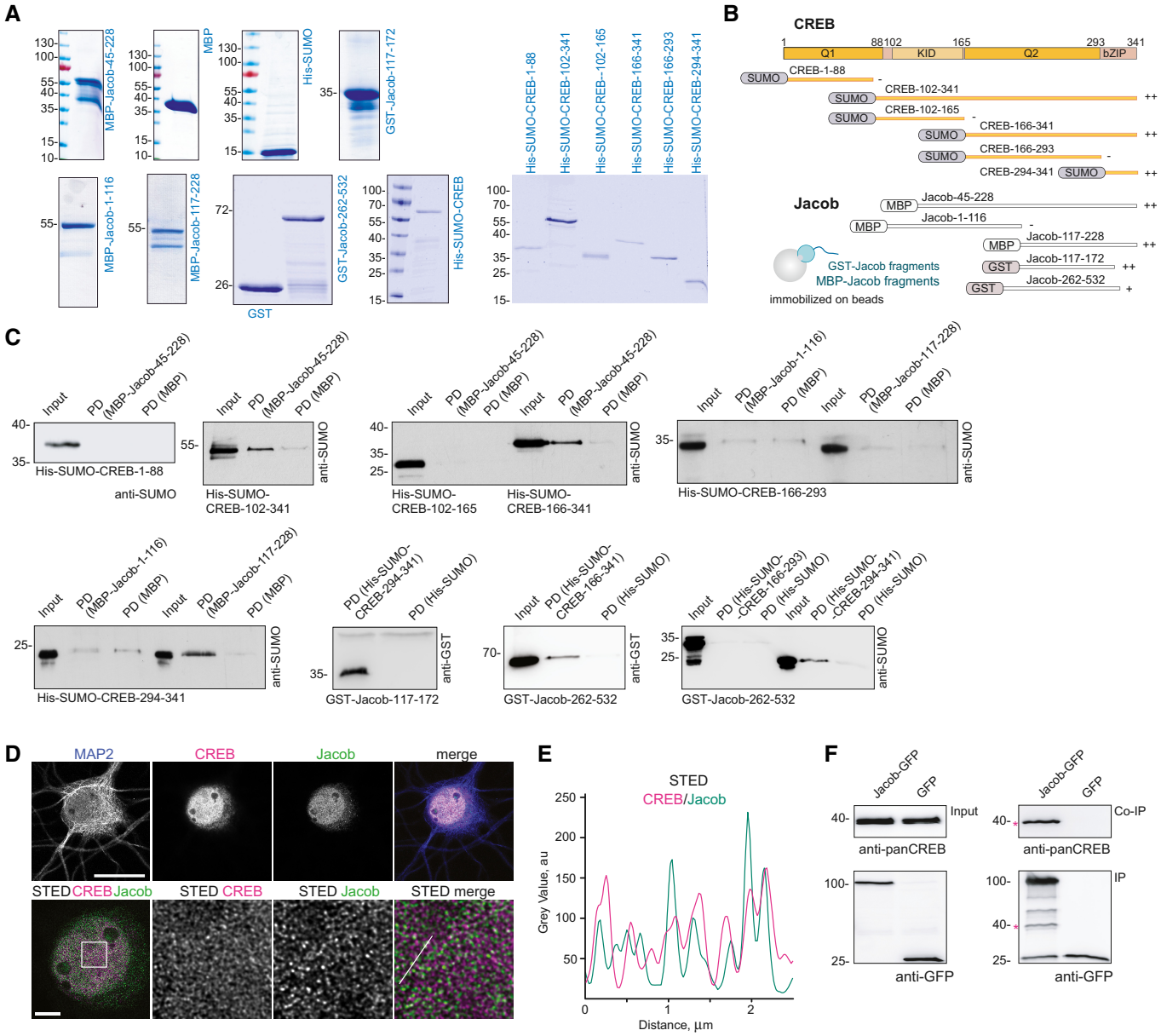

Figure EV2. Mapping of the binding interfaces between Jacob and cAMP-responsive element-binding protein (CREB).

A Coomassie blue staining depicting the purity of bacterially produced proteins used for pull-down assays between CREB and Jacob.

B Scheme representing the constructs used for mapping of the interaction sites in Fig 1D and Appendix Fig S1B.

C The N-terminus of Jacob (117-172 aa in red) interacts with the bZIP domain of CREB, but not with the Q1 (1-88 aa), KID (102-165 aa), or Q2 (166-293 aa) domain. The C-terminus of Jacob (262-532 aa) shows weaker binding to the bZIP domain of CREB. Images of immunoblots representing pull-down assays performed with Jacob and CREB protein fragments depicted in the panel (B).

D, E Confocal and STED images show an association of CREB with Jacob in the nucleus of DIV16 hippocampal primary neurons. (D) The upper panel represents deconvolved confocal images. Lower panels depict deconvolved STED images. Scale bars: 20 and 5 µm, respectively. Inserts are denoted by a white square. (E) Line profiles indicate the overlap of relative intensities for CREB and Jacob along a 2.5 µm line.

F Endogenous CREB co-immunoprecipitate with overexpressed Jacob-GFP, but not GFP from HEK293T cell extracts. The asterisk denotes the CREB band from a membrane subsequently re-probed with an anti-GFP antibody.

Source data are available online for this figure.

© 2023 The Authors

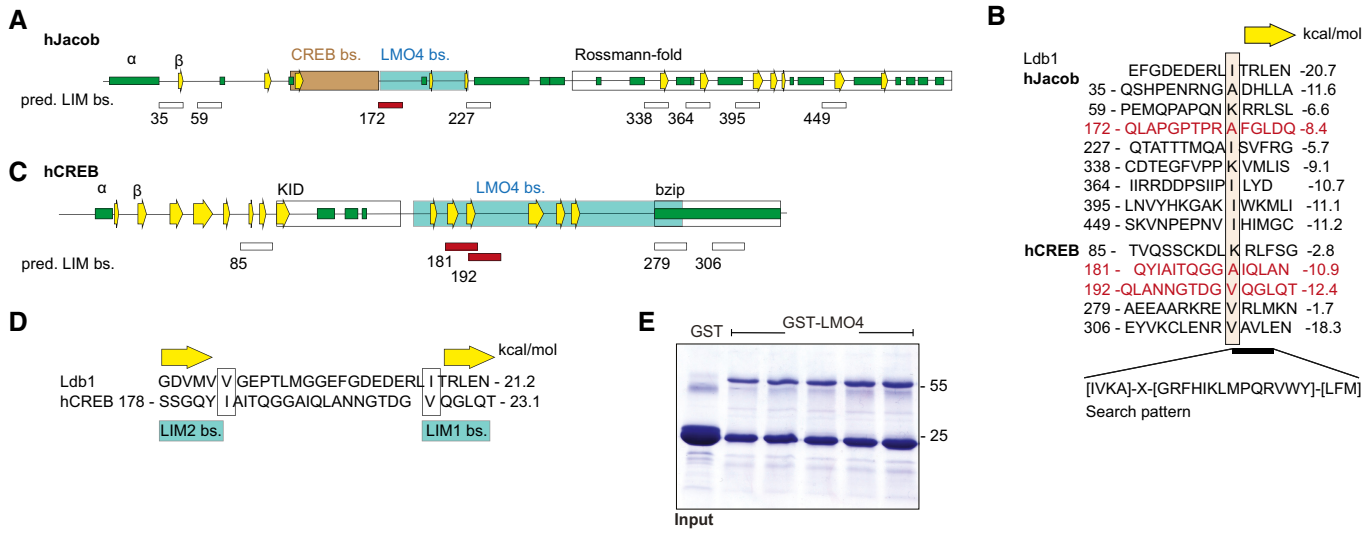

Figure EV3. Nitarsone disrupts the Jacob-LMO4 interaction.

A–D Predicted binding sites for LMO4 LIM domains in Jacob and cAMP-responsive element-binding protein (CREB). (A) Schematic structure of human Jacob showing predicted secondary structures (helices, green; β-strands, yellow arrows) and experimentally determined binding regions for CREB (orange) and LMO4 (gray). The C-terminus of Jacob is predicted to have a Rossmann-fold similar to caspases. (B) The LIM1 binding peptide of Ldb1 is aligned to 8 sequences of Jacob that match the search pattern for the conserved hydrophobic residues and the adjacent β-strand. Structures of LIM1:peptides were modeled and free energy ΔΔG were calculated. Only the peptide starting at 172 (red) lies within the LMO4 binding region. In human, CREB 5 matching peptides were identified. (C) Schematic structure of human CREB with labeled LMO4-binding region and known KID and bZIP domains. (D) The two peptides starting at 181 and 192 are within the LMO4-binding region and align to Ldb1 peptide where 181 binds to LIM2 and 192 to LIM1.

E Image of gels stained with coomassie blue showing the purity of bacterially produced GST-LMO4 used for pull-down assay.

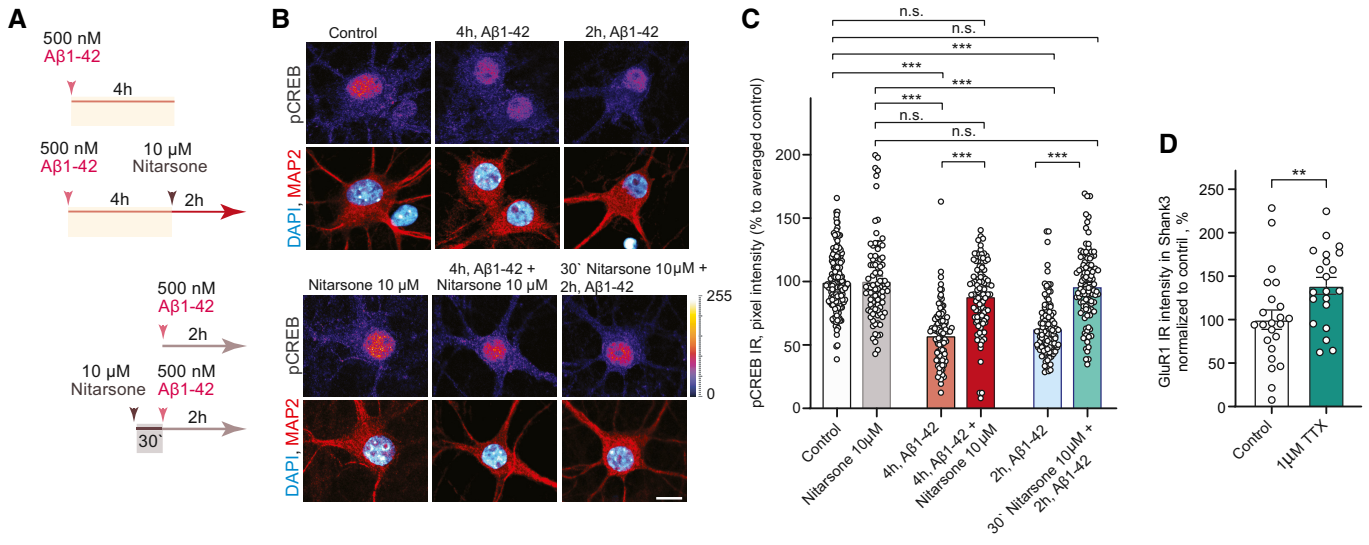

Figure EV4.

© 2023 The Authors

Figure EV4. Nitarsone prevents Aβ-induced cAMP-responsive element-binding protein (CREB) shutoff *in vitro*.

A–C Acute treatment with 10 μM Nitarsone rescues $Aβ_{1-42}$-induced CREB shutoff. (A) Scheme of the experimental design. The dissociated, hippocampal cell cultures at DIV16 were either pre-treated for 30 min with 10 μM Nitarsone and subsequently 2 h with 500 nM $Aβ_{1-42}$ or the drug was added 2 h after the 500 nM $Aβ_{1-42}$ treatment. The pCREB immunoreactivity was measured in comparison to vehicle control. (B) Representative confocal images of hippocampal neurons. Lookup table indicates the pixel intensities from 0 to 255. Scale bar: 10 μm. (C) Bar plot representing nuclear pCREB immunostaining intensity normalized to vehicle control. $N = 88–101$ from 5 to 7 independent cell cultures. $^{***}P < 0.001$ by two-way ANOVA with Sidak's *post hoc* test.

D Treatment with 1 μM TTX induced upregulation of GluR1 surface expression. $N = 21–23$ dendritic segments from three independent cell cultures. $^{**}P < 0.01$ by two-tailed Student's *t*-test.

Data information: All data are represented as mean ± SEM.
Source data are available online for this figure.

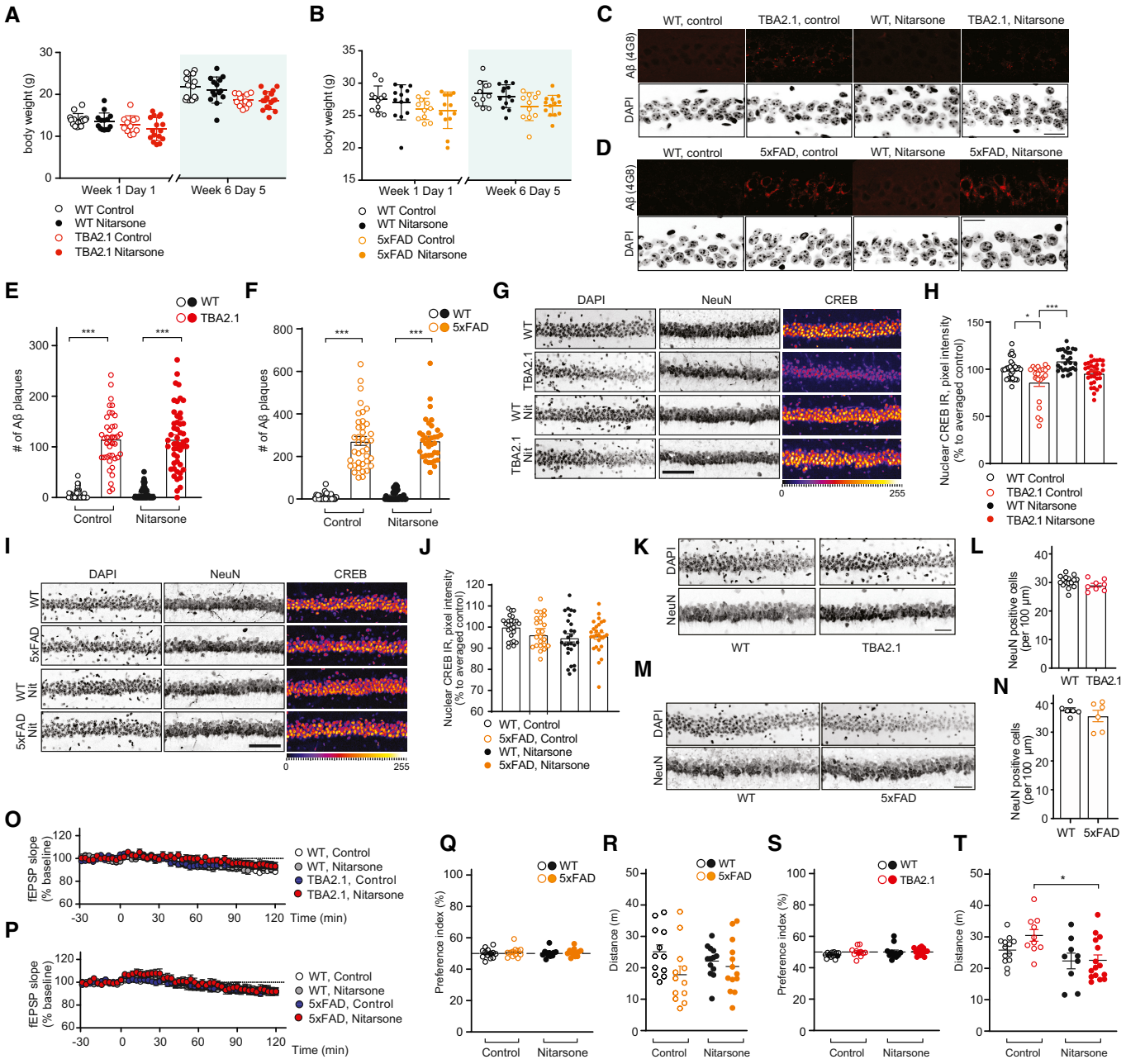

Figure EV5.

◀ **Figure EV5. Treatment with Nitarsone rescues Alzheimer's disease (AD)-related phenotypes *in vivo*.**

A, B Nitarsone treatment did not affect body weight of (A) TBA2.1 (N = 22–24 animals per group) or (B) 5xFAD mice (N = 11–13 animals per group).

C–F Nitarsone treatment does not change amyloid load in (C, E) TBA2.1 and (D, F) 5xFAD mice. (C, D) Confocal images averaged from two sections of the molecular layer of CA1 labeled for amyloid-β (4G8 antibody) and co-stained with DAPI. Scale bar: 100 μm. (E, F) Bar plots representing the number of amyloid-β-positive puncta. (E) TBA2.1 N = 40–50 CA1 regions 6–9 animals per genotype and (F) 5xFAD N = 33–40 CA1 regions 6–7 animals per genotype.

G, H Nitarsone rescues the reduction of CREB immunoreactivity in NeuN positive cells in CA1 of TBA2.1 mice. (G) Representative confocal images of CA1 cryosections from 11-week-old mice stained for NeuN, DAPI, and CREB. Scale bar: 10 μm. (H) Bar plot of CREB nuclear staining intensity. N = 21–34 hippocampal sections from 6 to 9 animals.

I, J Nitarsone does not affect CREB immunoreactivity in NeuN-positive cells in CA1 of TBA2.1 mice. (I) Representative confocal images of CA1 cryosections from 18-week-old mice stained for NeuN, DAPI, and CREB. Scale bar: 10 μm. (J) Bar plot of CREB nuclear staining intensity. N = 28–34 hippocampal sections from 6 to 7 animals.

K, L TBA2.1 mice do not display neuronal loss at the beginning of the Nitarsone treatment. (K) Representative confocal images of distal CA1 cryosections from 4 weeks old mice stained for NeuN, DAPI, and CREB. Scale bar: 10 μm. (L) Bar graph representing the average number of NeuN-positive cells normalized to WT treated with vehicle. N = 8–16 hippocampal sections from 2 to 3 animals.

M, N 5xFAD mice do not display neuronal loss at the end of the Nitarsone treatment. (M) Representative confocal images of distal CA1 cryosections from 19-week-old mice stained for NeuN, DAPI, and CREB. Scale bar: 10 μm. (N) Bar graph representing the average number of NeuN-positive cells normalized to WT treated with vehicle. N = 6 hippocampal sections from two animals.

O, P Basal synaptic transmission is not affected by bath application of Nitarsone in (O) TBA2.1 and (P) 5xFAD mice. TBA2.1: N = 14–18 slices from 5 to 6 mice and 5xFAD: N = 17–18 slices from six mice.

Q, R (Q) Nitarsone treatment does not influence preference index and (R) distance traveled during open-field arena exploration of TBA2.1 mice. N = 12–13 mice per group.

S, T (S) Nitarsone treatment does not influence preference in-dex and (T) slightly normalizes increased distance traveled during open-field arena exploration of 5xFAD mice. N = 12 mice per group.

Data information: $^{*}P < 0.05$, $^{***}P < 0.001$ by linear mixed-effects model followed by Tukey's multiple comparisons test. All data are represented as mean ± SEM.
Source data are available online for this figure.

© 2023 The Authors